Oral presentation, Int. Conf. On Ion Sources, 2021, 20-24 Sept, virtual (host: TRIUMF, Vancouver, Canada)

Optimization of ion transport in a combined RFQ Cooler with axial magnetic field

ID: 5

M. Cavenago*,[1], M. Rome[2], G. Maero[2], L. Bellan[1], F. Cavaliere[2], M. Comunian[1], A. Galata[1], M. Maggiore[1], N. Panzeri[2], A. Pisent[1], L. Pranovi[1], M. Sattin[1]

[1] INFN-LNL, viale dell'Universitá n.2 , 35020 Legnaro (PD) Italy, [2] Univ. of Milano, Dip Fisica, e INFN-MI, Milano, IT

1) Introduction

2) Setup: plugin; parts; applied voltage network; beam extraction

3) Ion transport theory and simulation results: ray tracing + diffusion; pencil emittance growth; energy spread

4) Conclusions.

Abstract: The accurate mass spectrometry (with resolution goal 1:20000) of exotic ions requests beams with low energy spread (goal is about 0.5 eVrms or lower) and low tranverse emittance; so it is necessary to cool ions produced by a spallation source by a factor from 5 to 10. In a radiofrequency (rf) quadrupole cooler (RFQC), collisions decrease ion kinetic energy, while rf and bias voltages confine and reaccelerate ions towards the extraction, where the cold ion beam is formed. Operation is based on carefully chosen voltage tunings, and among others: the dependence on ion species and gas pressure p_g, which requests an adequate pumping system; the difficult design of an efficient ion extraction, which critically depends on residual ion speed. Progresses in the experimental setup are described. Indications from simple ion tracing and ion+collision tracing are compared. Results are applied to a simple triode extraction system, and more flexible configurations are considered..

1.0) Introduction

Exotic ions (for nuclear research, see for example at LNL project SPES, Selective production of Exotic Species) are produced in hot ion source by spallation (for example fast protons impinging on uranium carbide). Their beams have: **1) low intensity 2) large energy spread (say 5 eV rms); 3) large emittance.**

To select one exotic species, we need to resolve its mass with high accuracy with a HRMS (High Resolution Mass Spectrometry) which requires an input beam with:

1) Low energy spread (0.5 eVrms); 2) low emittance

Principle of cooling:

1) Decelerate ions so that their collision with gas is more effective. Kinetic energy $K_i=m_i\ v^2/2$ down from 5 keV to 100 eV

2) Keep beam confined (for example with an RFQ)

3) Apply gas to get a friction force

$$F_r = -m_i \mathbf{v} \nu_m$$

where ν_m is the collisional rate with gas, say He. For K_i > few eV, we have $d(\nu_m |\mathbf{v}|)/dKi > 0$ so faster particle are dragged more → cooling

4) Apply a bias potential (of 10 V) so that all ions are refurbished with the same amount of energy

5) Extract and reaccelerate ions

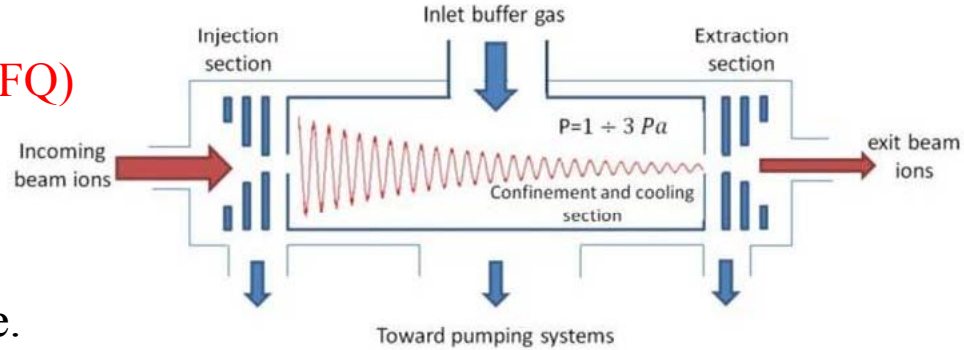

Traditional scheme of RFQ Cooler: slowed ions enter in a gas cell with a large oscillation, confined by a RFQ; gas friction reduces oscillations; ions exit gas cell are accelerated again

RFQ = radiofrequency quadrupole

RFQC = RFQ cooler

1.0) Introduction

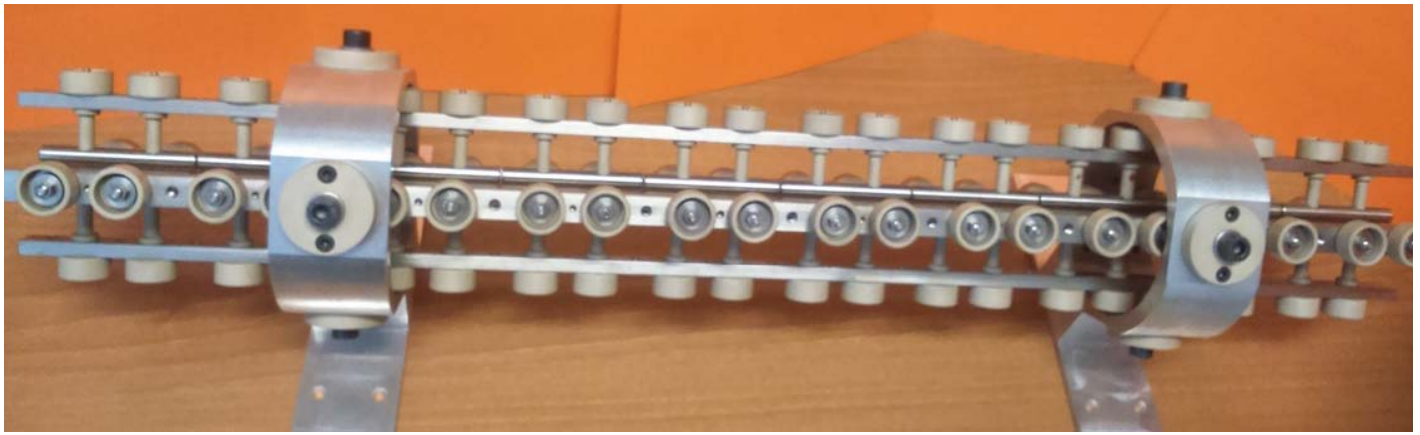

LNL prototype RFQC1: 9 gaps (2 mm wide) separate device into 10 sections or cells, with few Volts potential difference among them

Mixed confinement: a magnetic confinement is added to the radio-frequency quadrupole confinement.

This can be tested by inserting RFQC1 into a solenoid, e.g. the high precision solenoid of the Eltrap test facility, with an emittance meter EMI and Faraday cups FC (see scheme b).

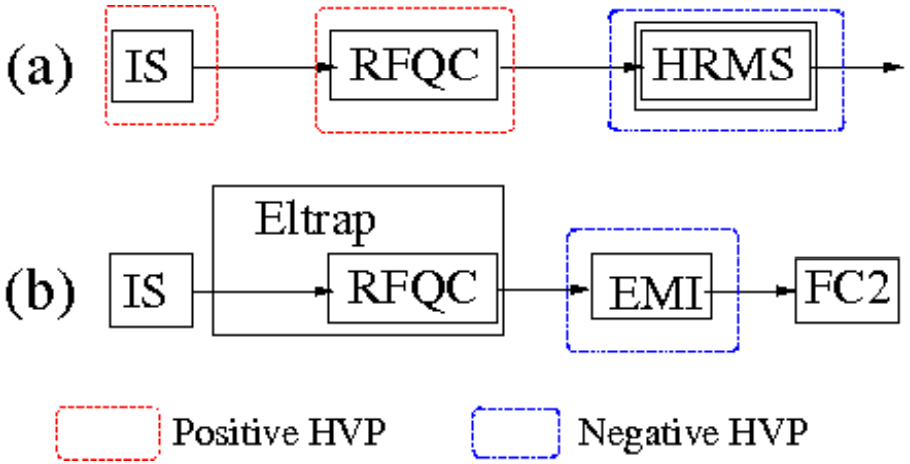

Comparison between (a) accelerator setup (b) Eltrap setup scheme (Fig 1 in Ref[7])

2 Setup of Eltrap+ RFQC

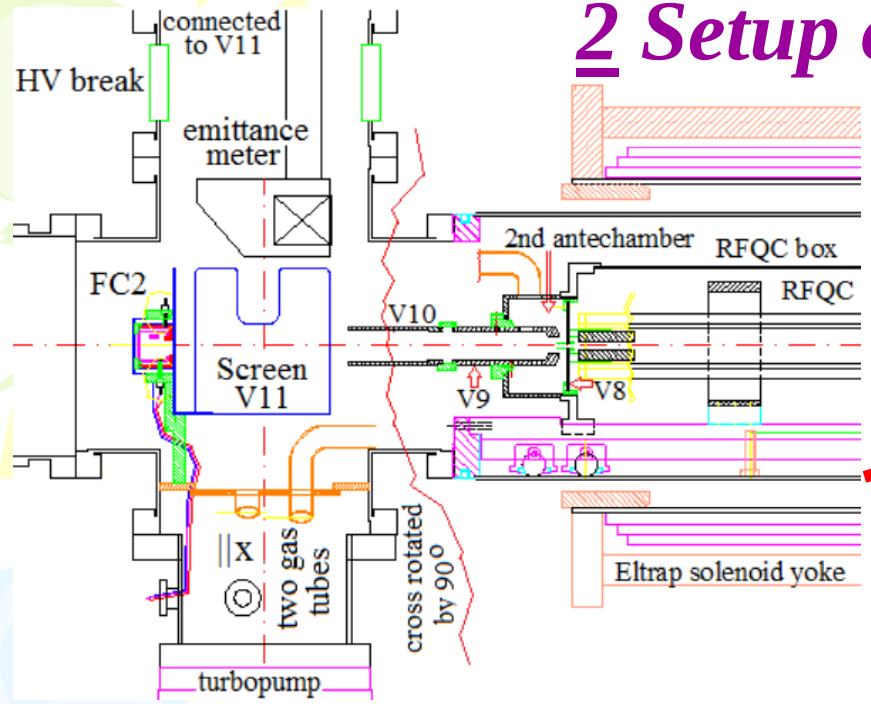

Extraction (Fig 3 in Ref[7]: Cavenago et al RSI 2019)

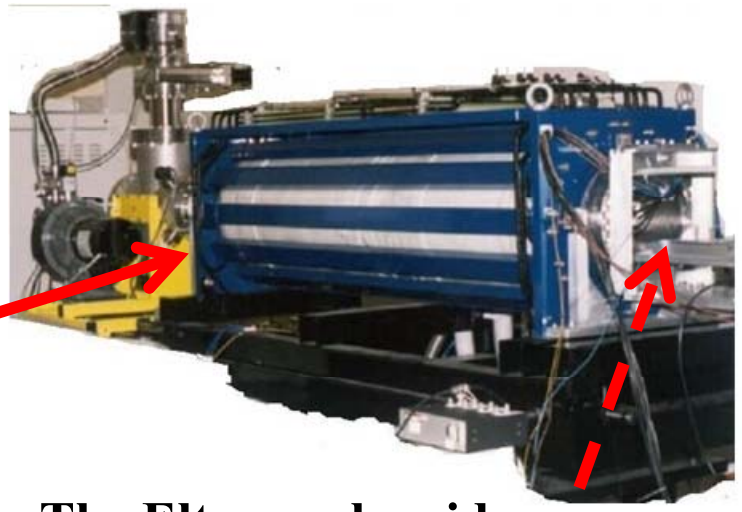

The Eltrap solenoid, with flange for plugin insertion (dashed arrow)

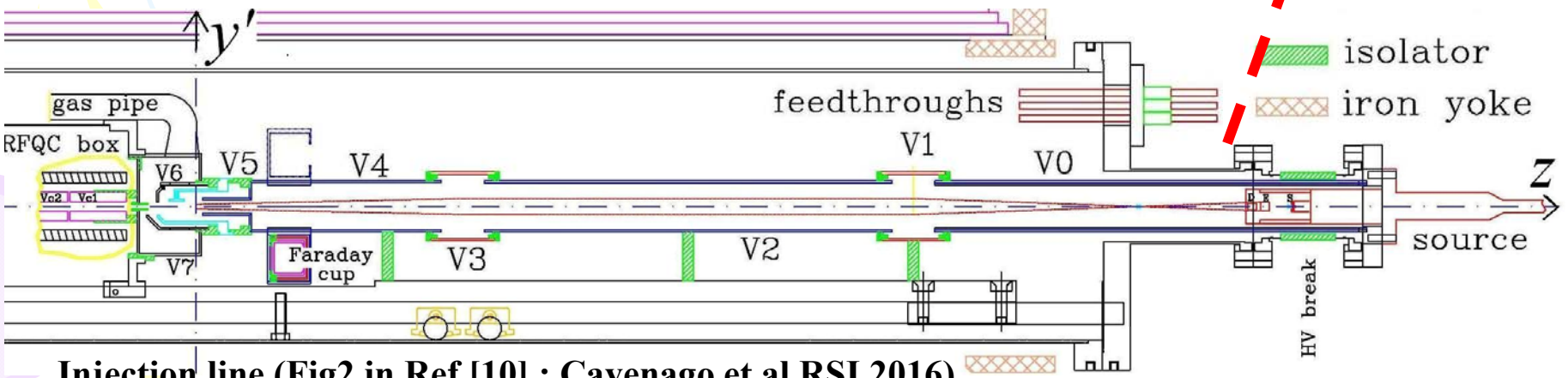

Injection line (Fig2 in Ref [10] : Cavenago et al RSI 2016)

Plug-in

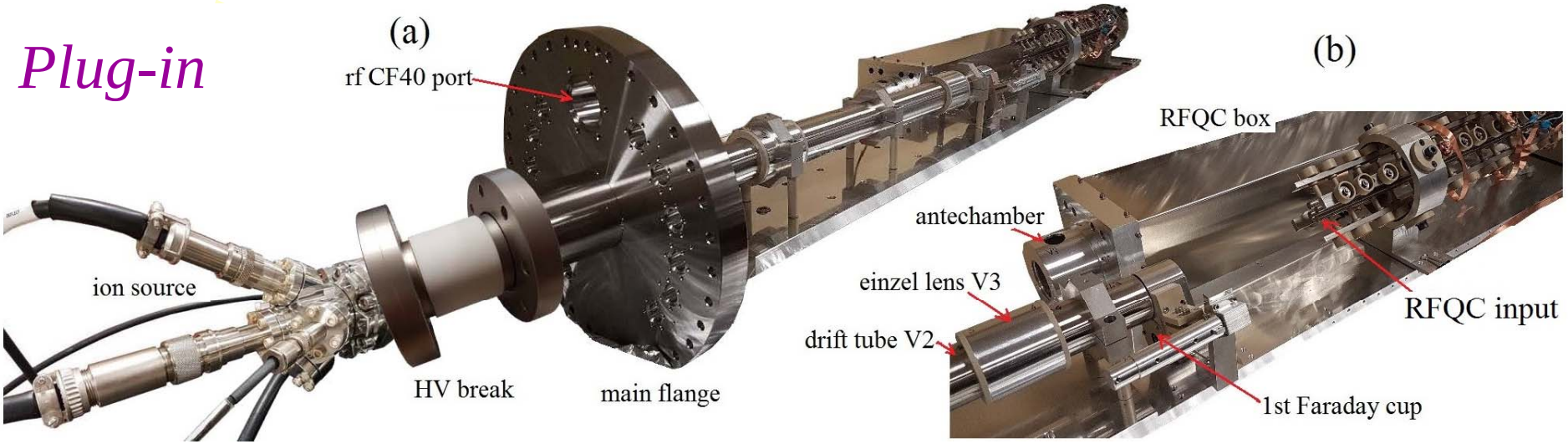

Figure: (a) the plugin with most components shown; (b) zoom on the 1st Faraday cup and the RFQC input; box moved aside

Faraday cup FC1 (right) ; note the drift tube (left): FC1 replace drift tube with a simple rotation

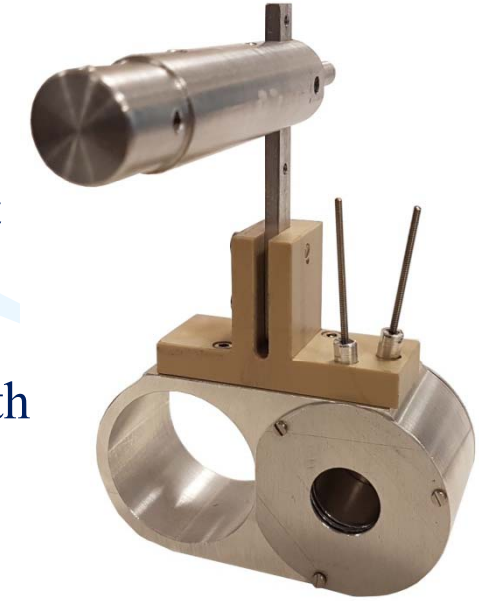

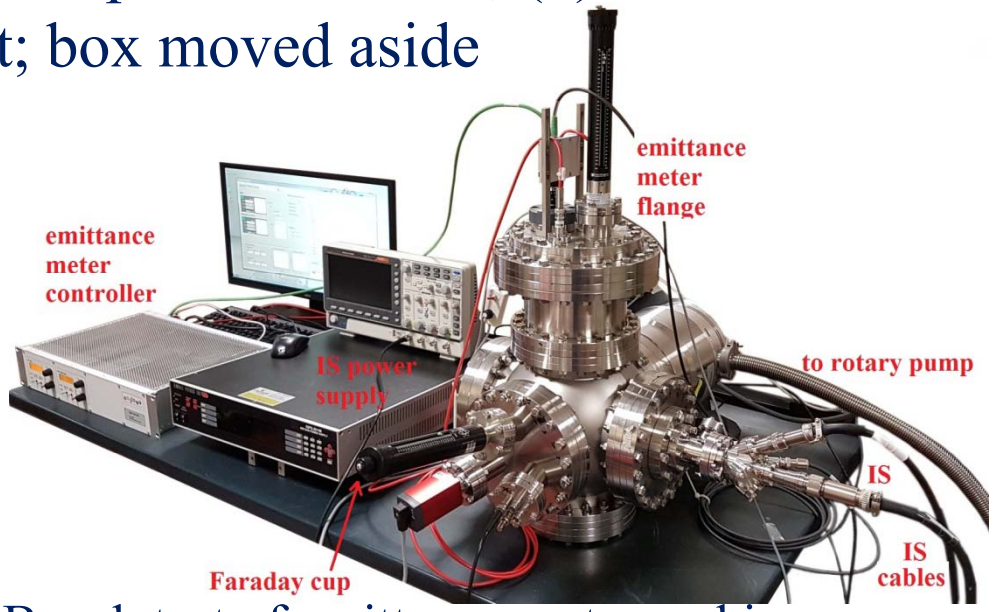

Bench test of emittance meter and ion source; a different faraday cup was used

Applied bias potentials (static i.e. frequency zero = DC)

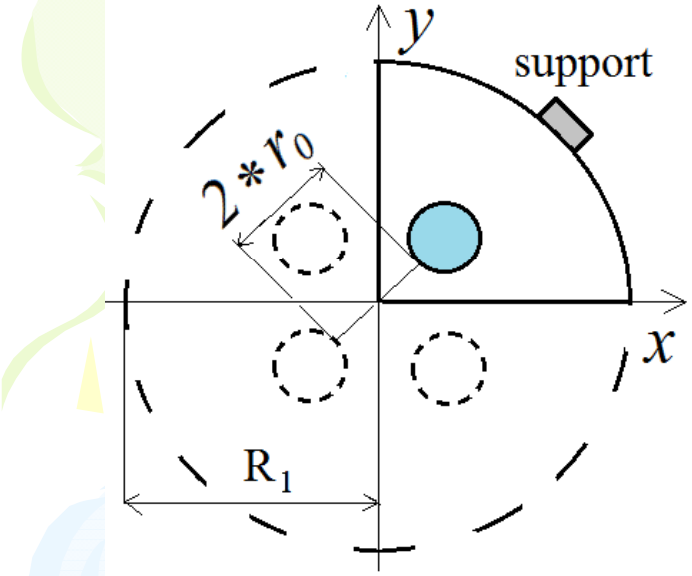

RFQC xy cross section

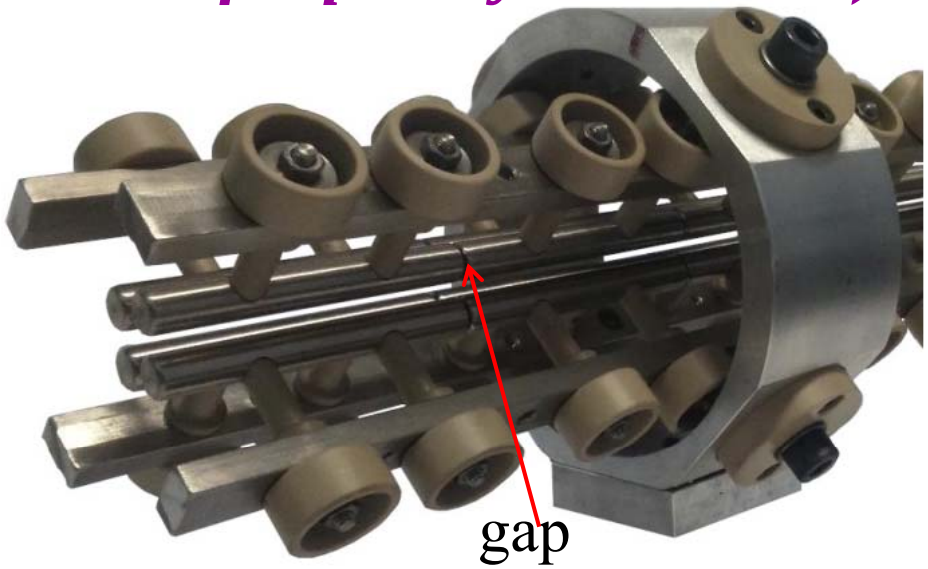

RFQC end: note each electrode has two support points.

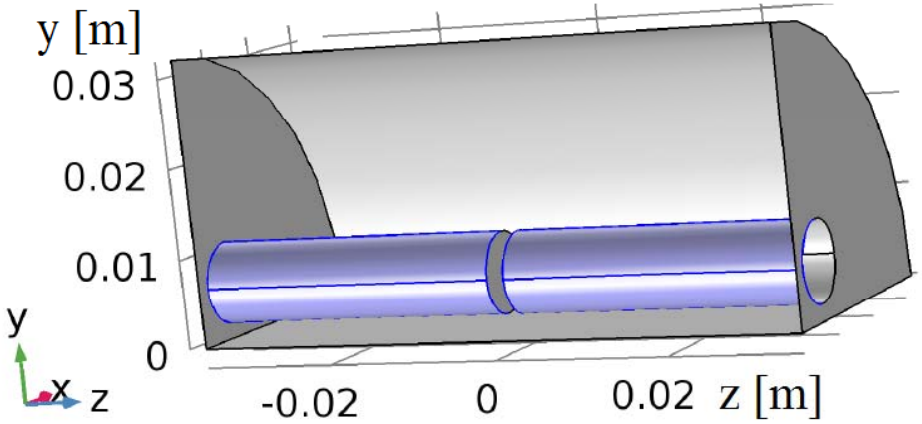

Simulation geometry for a basic cell: one gap and the 2 halves of adjacent electrodes

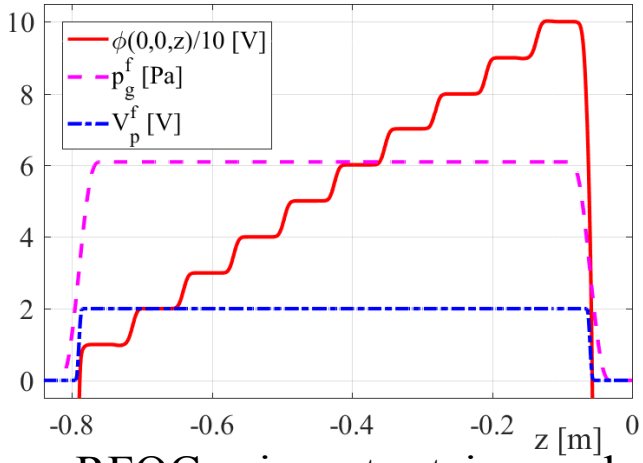

DC voltage on RFQC axis: note stairway shape. Applied gas (and rf) profiles also shown [7]

Network for radiofrequency and DC voltages

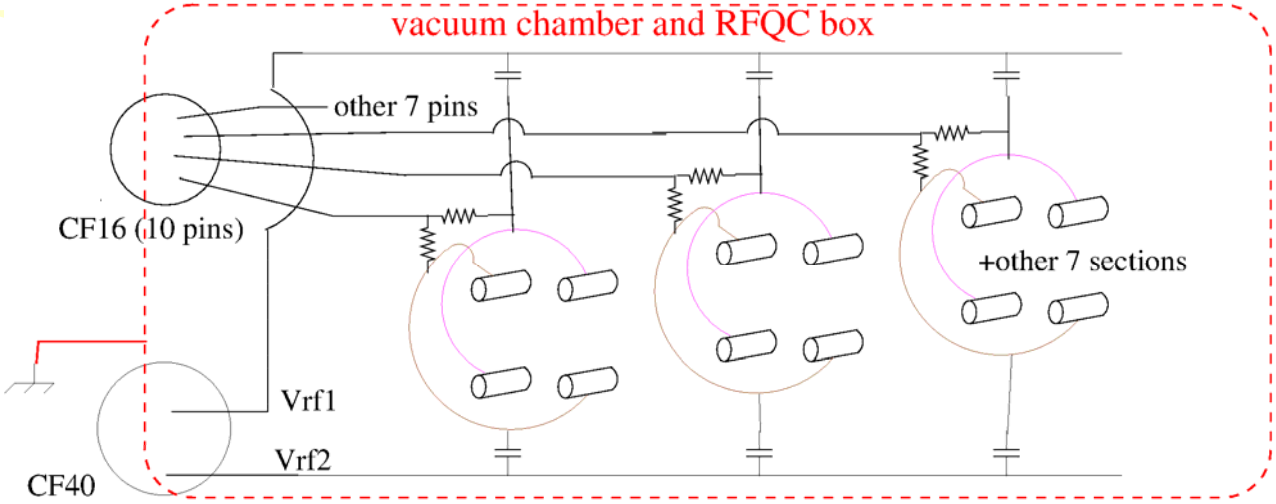

Multiplexer: the 40 electrodes require only 12 inputs on the plug-in vacuum flange

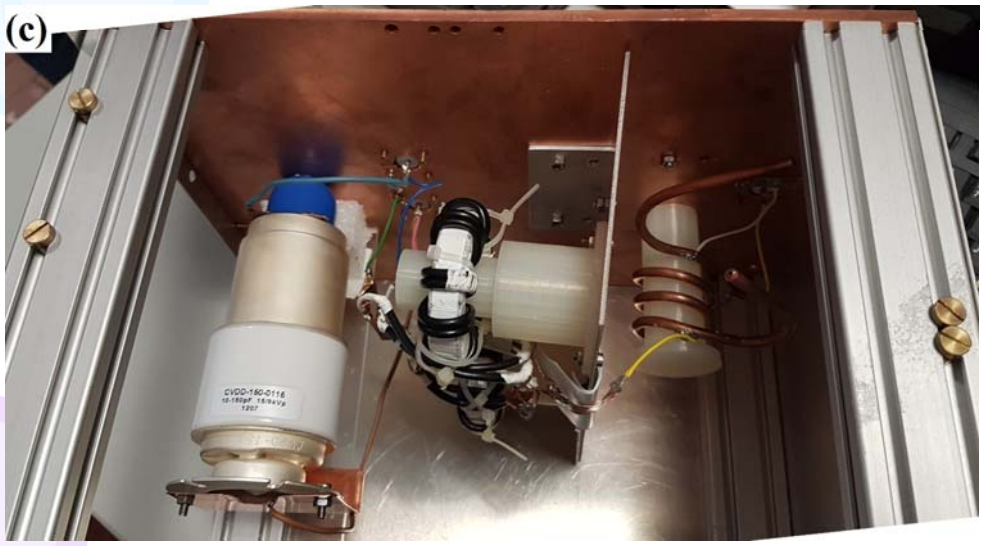

Medium power matching box (cover removed)

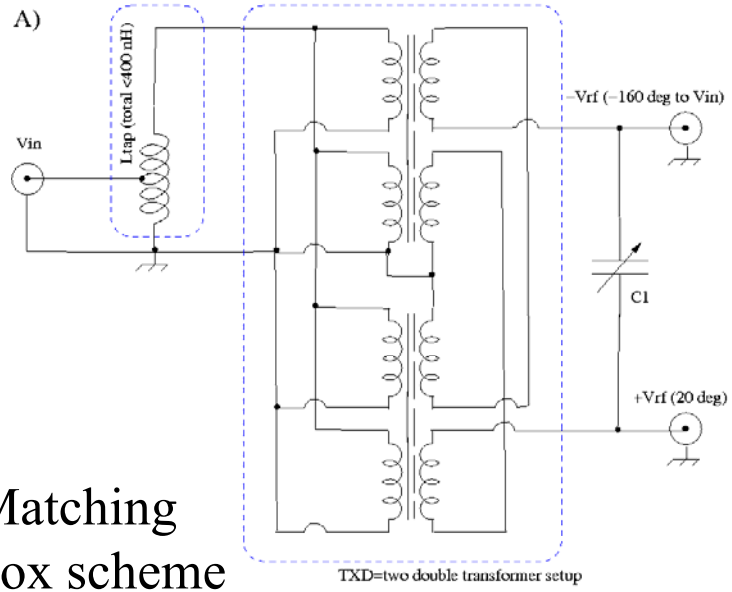

Matching box scheme

Extraction, and gas pipes/pumps

The RFQC box can be filled to 9 Pa He (for short times, due to gas economy); escaping gas is collected by antechambers A1,A2 and piped to pump V551

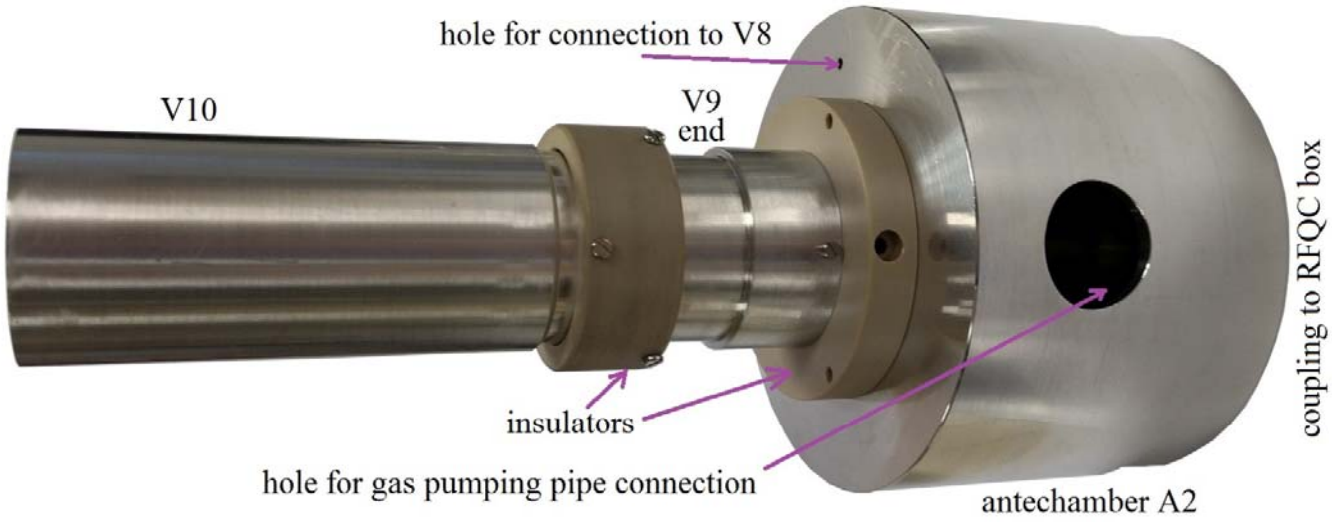

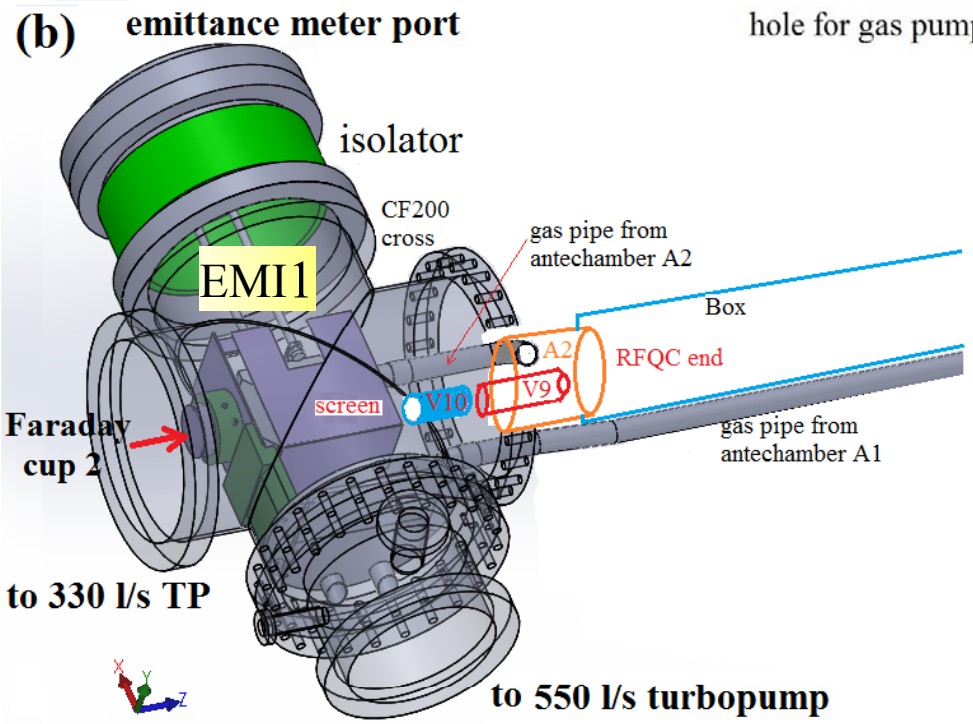

The triode assembly: it is cantilevered by the RFQC box, rigidly fixed to the plugin, and thus to the ion source.

(b) The emittance Meter EMI1 and Faraday cup FC2 <u>are not fixed to plugin</u>, but to a CF200 cross. When EMI1 is retracted, beam will still propagate in a screened area at a controlled voltage, until stopped by FC2. The gas pipe from A1 has bayonet-stile junction.

3 Ion transport into the RFQC

We have DC and rf fields, and collisions. DC field and potential are easily solved

$$\mathbf{E}_s = -\nabla\phi_s \qquad \phi_s = V_n^c \ (\text{with } n = 1, ...10)$$

(given the applied potentials V^c_n) and near axis z, they are approximately axially symmetric

Rf potential has a quadrupole pattern

$$\mathbf{E}_f = -\nabla\phi_f \qquad \phi_f \cong 2V_{rf}(xy/r_0^2)\cos\omega t$$

$$\omega \cong 2.5 \times 10^7 \text{ rad/s}$$

Macromotion approximation

To simplify motion calculation we average on each rf period (250 ns at 4 MHz): resulting motion is called macromotion[2,3,13], with macromotion frequency and cyclotron frequency (both less than 100 kHz in our case)

$$\omega_M = \frac{e}{m_i\sqrt{2}}\frac{V_{rf}}{\omega r_0^2} \quad , \quad \Omega_i = \frac{e|B^s|}{m_i}$$

Macromotion is driven by the so-called ponderomotive force $\mathbf{F}_p \equiv e\mathbf{E}_p = -e\nabla\phi_p$

with approximately axially symmetric potentials $\phi_p \cong (m_i/2e)\omega_M^2(x^2+y^2)$

Collision 1st effect: friction force

$F_r = -m_i\mathbf{v}\nu_m$ ν_m is the collision frequency (depending on ion speed)

Collision 2nd order effect: straggling = diffusion = fluctuation

We add random kicks $m_i \eta$ to the friction force, obtaining the Langevin equation

$$\mathrm{d}_t \mathbf{v} = \frac{e}{m_i}\left(\mathbf{E}_s + \mathbf{E}_p + \mathbf{v} \times \mathbf{B}^s\right) - \nu_m \mathbf{v} + \boldsymbol{\eta}$$

$$\langle \boldsymbol{\eta} \rangle = 0 \quad , \quad \langle \eta^m(t)\eta^n(t') \rangle = D^{mn}\delta(t-t')$$

Here m,n=1,2,3=x,y,z and $\langle\ \rangle$ indicates the statistical average. By definition of random, kick average is zero.

The second correlation of kicks is specified by the diffusion tensor D, calculated from inter-atomic potentials [2,7,14]; we assume that higher order correlations are normally distributed.

From ray to pencil approximation

Since $m_i/m_t >> 1$ with m_t the mass of gas (e.g. $m_i/m_t = 133/4$ for Cs against He) each collision slightly deviates Cs^+ ion, and we can still speak of average trajectory (short name: ray), around which a set of fluctuations (short name: pencil) develops (and hopefully damps)

Ray: $\bar{x} = \langle x \rangle$ **Fluctuations:** $\tilde{x} = x - \bar{x}$

Most of all, we define new variables a,b,c (the second moments of fluctuation)

$$a_{mn} = \langle \tilde{x}^m \tilde{x}^n \rangle \quad , \quad b_{mn} = \langle \tilde{v}^m \tilde{v}^n \rangle \quad , \quad c_{mn} = \langle \tilde{x}^m \tilde{v}^n \rangle$$

They evolve as from Langevin eq. and the symmetry of D. For diagonal D, linearized eq. are

$$d_t b_{xx} = 2(D^{xx} - \nu_m b_{xx} - \psi_{,xx} c_{xx}) \qquad \psi = e(\phi_s + \phi_p)/m_i$$

(continues from prev. slide)

$$d_t a_{xx} = 2c_{xx} \quad , \quad d_t c_{xy} = -\Omega_i c_{xx} - \nu_m c_{xy}$$ (initial values are zero)

and so on and similarly for z [14]; xx=yy; zero correlations were omitted. The correlation c_{xy}=-c_{yx} is not zero because of the applied magnetic field, coupled to c_{xx} and damped as shown above.

Reminder: for reference here V_0=-4800 V, K_i is the kinetic energy (5 keV at source exit), V_s is the source voltage wrt ground, H is the Hamiltonian (decreased by collisions), H_i its initial value about H_i=e V_s and h is the reduced Hamiltonian

$$h = H/m_i = \tfrac{1}{2}\mathbf{v}^2 + (e\phi_s/m_i) \qquad V_s = K_i/e + V_0 = 200 \text{ V}$$

The pencil emittance (normalized, rms)

The quantity

$$\epsilon_x^p = \sqrt{a_{xx}b_{xx} - c_{xx}^2 - c_{xy}^2}$$

which has the dimension of m^2/s can be called pencil emittance because: 1) when no axial magnetic exists, it reduces to the rms normalized emittance (apart from constants, and relativistic factors); 2) with or without magnetic field, it evolves as

$$\mathrm{d}_t(\epsilon_x^p)^2 = 2a_{xx}D^{xx} - 2\nu_m(\epsilon_x^p)^2$$

Thus, it is invariant when no gas exists (as emittance must behave); 3) since it is defined by fluctuations, its initial value is zero; to this, we should add ray tracing estimated emittance. Since D and ν_m change with K_i, for slow changes ε_x^p equilibrium value is

$$(a_{xx}D^{xx}/\nu_m)^{1/2}$$

With v_z the beam axial velocity, the geometric pencil emittance is defined as $\epsilon_{geo}^p \equiv \epsilon_x^p/|v_z|$

Diffusion adds more divergence to ray tracing estimates

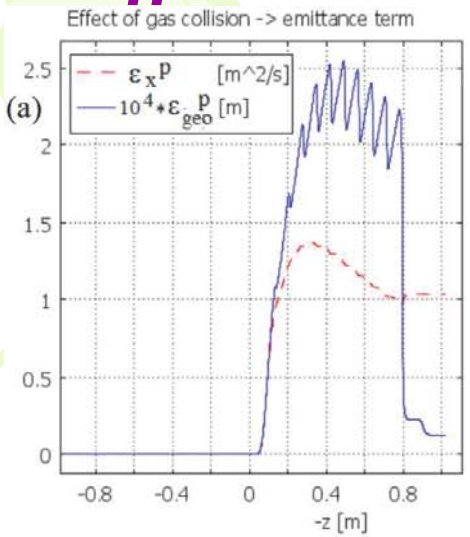

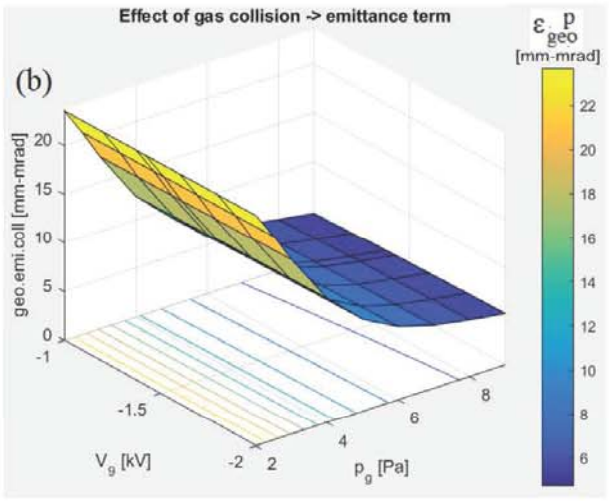

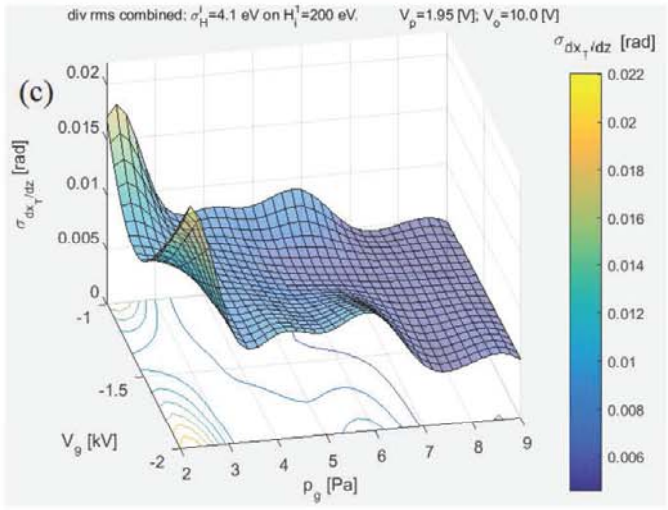

(a) Pencil emittance growth (and damping) by gas collisions: ε_x^p vs -z (abscissa reversed); also plotted $\varepsilon_{geo}^p = \varepsilon_x^p / |v_z|$; (b) output value of ε_{geo}^p ; (c) Preliminary results for output value of rms divergence

We scan both gas pressure p_g (maximum 9 Pa) and lens voltage V_9

Ray tracing still applies for $\bar{x}$ but now is not the only contribution to emittance and divergence!! Diffusion (fig b) adds up; so effects of good optics (V_9=-1.4 kV) are still visible in the total divergence (fig c), but comparatively reduced

(to do: beam redefinition when diffusion exceeds limits)

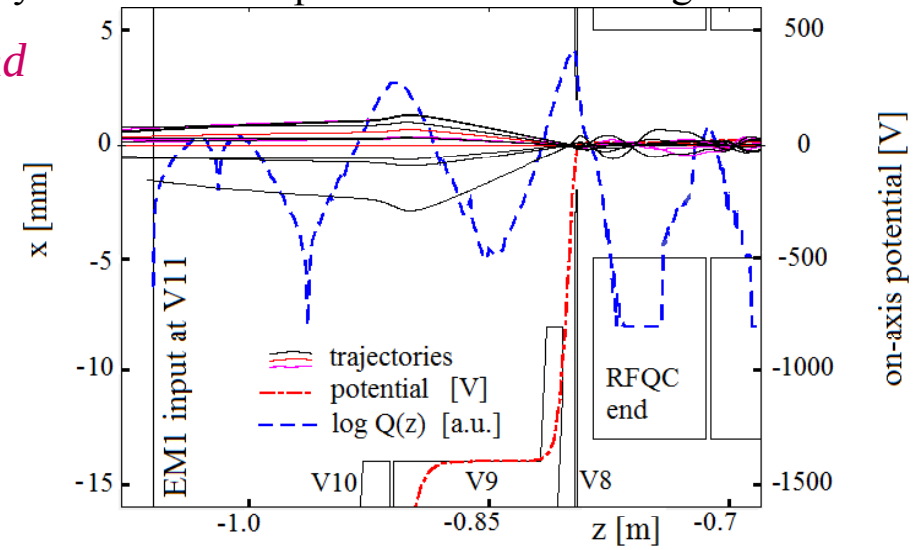

Ray tracing, as Fig 7 in Ref [7]

Energy spread

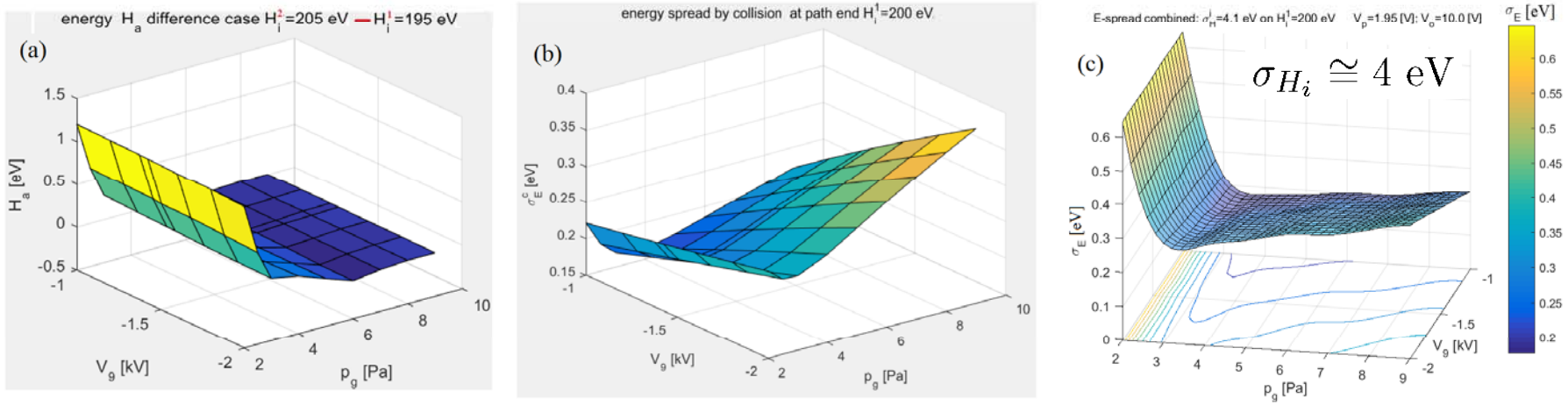

(a) difference of average final energies H_a vs gas pressure p_g and lens voltage V_9 for two H_i values (205 and 195 eV); b) rms fluctuation induced by gas collisions; (c) combined rms energy spread at output (assuming 4 eV at input).

For the energy spread, we have a different balance of effects with p_g

The energy fluctuations (see Fig. b) induced by collisions increase with p_g; but at low pressures (see Fig. a) the RFQC length is too short to clear the memory of the initial energy spread (assumed 4 eV rms). Other minor effects exist: since the rays follow slightly different paths, energy damping is slightly different. **Combination of all discussed effects (see fig c) shows that the requirement**

Rms(energy spread) < 0.4 eVrms **(factor 10 reduction from input)**

is safely met in a wide range including p_g from 3 to 9 Pa

4) Conclusions

The plan for completing the electronics and the differential pumping of the LNL RFQC prototype test into the Eltrap facility solenoid (University of Milano) is still progressing (but with hindrances from the present emergency situation). Theoretical tools to add the straggling effects of collisions into relatively fast ray tracing simulations were successfully implemented: results for triode configuration show good cooling of energy spread even at reasonable gas pressure $p_g > 3$ Pa, while divergence cooling requires larger p_g ($>$ 6 Pa); so optimization of other configurations is worthwhile investigating.

Thanks for your attention!

[1] Comunian M. et al. (2020) J.Phys.Conf.Ser. **1401**, 012002
[2] Schwarz S, (2006) Nucl. Instrum. Meth., **A 566** 233 .
[3] Herfurth F, et al, 2001, *Nucl. Instrum. Meth. Phys. Research*, **A469**, 254.
[4] Maggiore M et al. , (2014) *Rev. Sci. Instrum.* **85**, 02B909; doi: 10.1063/1.4830357
[5] Amoretti M. et al., 2003 Rev. Sci. Instrum. **74**, 3991.
[6] Guo-Zhong Li and G Werth, (1992) *Phys. Scr.* **46**, 587.
[7] M. Cavenago, et al., (2019) Rev. Sci. Instrum. **91**, 113334 .
[8] M. A. Lieberman and A. J. Lichtenberg, 1994 *Principles of Plasma Discharges and Material Processing*, John Wiley, New York, especially chapter 4.
[9] R. Boussaid, G. Ban, G. Quéméner, Y. Merrer, and J. Lorry, 2017, Phys. Rev, ST-AB **20**, 124701.
[10] Cavenago et al., 2016 Rev. Sci. Instrum. **87**, 02B504.
[11] Cavenago M et al., pp 3626-3630, in *9th Int. Particle Acc. Conf., IPAC18*, online at www.jacow.org;
[12] Barqucst B R ct al., pp 3914-3916, as Rcf. [11]
[13] Moore R B, Gianfrancesco O, Lumbo R, Schwarz S, Int. J. Mass Spectr., **251** 190 (2006).
[14] Cavenago M., unpublished.